TOPICAL REVIEW — Iron-based high temperature superconductors

Optical spectroscopy studies on $FeTe_{1-x}Se_x$ and $A_xFe_{2-y}Se_2$ (A = K, Rb, Cs): A brief overview

Yuan Rui-Hua(原瑞花) and Wang Nan-Lin(王楠林)†

Institute of Physics, Chinese Academy of Sciences, Beijing 100190, *China*

(Received 14 June 2013)

In this short overview, we summarize the optical spectroscopy studies on iron selenide superconducting systems $FeTe_{1-x}Se_x$ and $A_xFe_{2-y}Se_2$. We elaborate that optical spectroscopy measurements yield fruitful information about the band structure evolution across the AFM phase transition temperature, the electronic correlation effect, the superconducting pairing energy gap, the condensed carrier density or penetration depth, the inhomogeneity and the nanoscale phase separation between superconductivity and antiferromagnetism in those systems.

Keywords:

PACS: 74.25.Gz, 74.70.–b, 74.62.Bf

DOI: 10.1088/1674-1056/22/8/087404

1. Introduction

The discovery of iron-based superconductors has attracted a great deal of interest in condensed matter physics community since 2008.[1] Similar to the cuprate compounds, the iron-based materials adopt a layered structure, and the essential structure unit is $Fe_2(As/Se)_2$ tetrahedron. As the simplest materials in the iron-based family, the 11 structural type FeTe/Se system consists of only $Fe_2(Te/Se)_2$ tetrahedron layers.[2] Bulk FeSe is a superconductor with $T_c \sim 8$ K. With Te doping, T_c could be enhanced to 15 K in $FeTe_{1-x}Se_x$ ($x \sim 0.5$).[3] Under high pressure, the superconducting transition temperature of FeSe could be raised to 37 K.[4] Recently, it is found that the single layer FeSe thin film grown on $SrTiO_3$ by molecular beam epitaxy (MBE) has a onset critical temperature over 50 K.[5] On the other hand, the other end member of the system, $Fe_{1+y}Te$ (usually with excess Fe, $y \neq 0$), has a bi-collinear antiferromgnetic (AFM) structure, and is usually considered as the parent compound of the system. $A_xFe_{2-y}Se_2$ (A = K, Rb, Cs) is another interesting Fe-chalcogenide based superconducting system whose superconducting temperature T_c can reach 32 K at ambient pressure[6] and up to 48 K under high pressure.[7] Those compounds can be viewed as intercalating alkaline metal into FeSe layer. However Fe vacancies are usually present in those compounds.[8] The physical properties of $K_xFe_{2-y}Se_2$ are much different from the FeAs-based systems. Neutron diffraction measurements revealed a novel block antiferromagnetic state with a very large ordered moment for $K_{0.8}Fe_{1.6}Se_2$.[9] ARPES experiments on the superconducting compound revealed an absence of the hole pocket at the Fermi level.[10] Furthermore, it is found that the superconductivity is very close to an insulating phase.

Optical spectroscopy is a powerful experimental tool in exploring the electronic structure and correlation effect in a quantum material. Here we present a short overview on the infrared study of $FeTe_{1-x}Se_x$ and $A_xFe_{2-y}Se_2$ systems. The contents include the normal state properties, the superconducting energy gap, the inter-plane optical response, the electronic correlation effect, inhomogeneity and nanometer phase separation, and magnetic transitions for the two type compounds.

2. $FeTe_{1-x}Se_x$

The first infrared study of the in-plane conductivity of $FeTe_{1-x}Se_x$ was reported by Chen *et al.*[11] The single crystal sample used in that work has the composition of $Fe_{1.05}Te$, which undergoes a first order structural phase transition at ∼65 K along with the bicollinear AFM order. Figure 1 shows the temperature dependences of optical reflectance $R(\omega)$ and optical conductivity $\sigma_1(\omega)$. The $R(\omega)$ spectra display a weak temperature dependence between 70 K and 300 K. The low frequency $R(\omega)$ decreases slightly with decreasing temperature. However, below 70 K, the low frequency $R(\omega)$ increases with decreasing temperature. Correspondingly, the low frequency conductivity decreases slightly with decreasing temperature from 300 K to 70 K. The spectra are rather flat without showing a clear Drude-like response. Since the width of the Drude component is the scattering rate of the charge carriers, the flat spectral structure indicates that the charge carriers experience rather strong scatterings or they have extremely short lifetimes. In this case, one would expect an absence of the well-defined quasiparticles. Below the structural/magnetic transition temperature of 65 K, a narrow Drude-like peak develops in $\sigma_1(\omega)$, indicating clearly a metallic response. Different from FeAs-based parent compounds where spin density wave (SDW) energy gaps develop below structural/magnetic

†Corresponding author. E-mail: nlwang@iphy.ac.cn

© 2013 Chinese Physical Society and IOP Publishing Ltd

transition temperatures,[12] no clear signature of the SDW gap formation is observed for the $Fe_{1.05}Te$ system. The same conclusion was also obtained subsequently by ARPES measurements on $Fe_{1.05}Te$.[13]

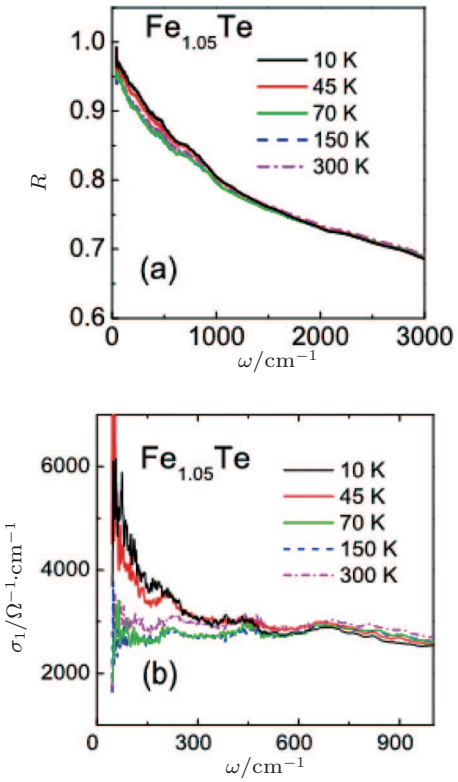


Fig. 1. (a) Optical reflectance and (b) conductivity spectra at different temperatures for $Fe_{1.05}Te$.[1]

The formation of a pairing energy gap in the excitation spectrum is an important property of a BCS superconductor. A threshold in the dissipative part of the conductivity spectrum at $\omega = 2\Delta$ could be observed in dirty superconductors $(1/\tau \geq 2\Delta)$ at $T \ll T_c$. The in-plane optical result of superconducting $FeTe_{0.55}Se_{0.45}$ single crystal was reported by Homes *et al.* (Fig. 2).[14] Figure 2 shows the temperature dependence of the real part of the optical conductivity of $FeTe_{0.55}Se_{0.45}$. The far-infrared region is shown in the inset. At room temperature, the conductivity is relatively flat and structureless, except for a sharp feature associated with the infrared-active Eu mode at 204 cm^{-1} which is due to the in-plane displacements of the Fe–Te/Se atoms. As the temperature is lowered, there is a redistribution of the spectral weight from high frequency to low frequency. This corresponds to a decrease of the scattering rate with decreasing temperature. The plasma frequency estimated from the Drude–Lorentz analysis is about $\omega_{p,D} = 7200$ cm^{-1}.

Below T_c, there is a dramatic suppression of the low-frequency conductivity. The loss of spectral weight is associated with the formation of a superconducting condensate, whose strength may be calculated from the Ferrell–Glover–Tinkham sum rule $\int_0^{\omega_c}[\sigma_1(\omega,T) > T_c - \sigma_1(\omega, T \ll T_c)]\,d\omega = \omega_{p,s}^2/8$. Here, $\omega_{p,s}^2 = 4\pi n_s e^2/m^*$ is the superconducting plasma frequency, and the cut-off frequency $\omega_c \sim 150$ cm^{-1} is chosen so that the integral converges smoothly. The sum rule yields $\omega_{p,s} = 3000 \pm 200$ cm^{-1}, corresponding to an effective penetration depth $\lambda_0 = 5300 \pm 300$ Å. The value is in good agreement with the recent tunnel-diode measurement on $FeTe_{0.63}Se_{0.37}$.

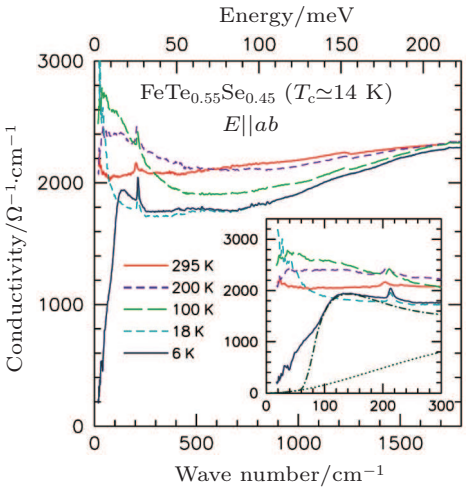


Fig. 2. Optical conductivity spectra at different temperatures, the inset shows the spectra at the far-infrared region.[14]

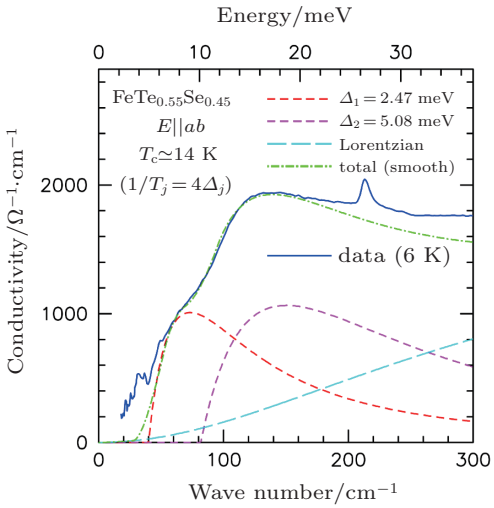


Fig. 3. Conductivity spectrum at 6 K for $FeTe_{0.55}Se_{0.45}$ together with calculations using a Mattis–Bardeen formalism for the contribution from the gapped excitations and a mid-infrared component.[14]

The conductivity spectrum at 6 K has been modeled quite well with the Mattis–Bardern formalism as shown in Fig. 3. A two-gap feature appears at 20 cm^{-1} (2.5 meV) and 41 cm^{-1} (5.1 meV), which is consistent with the ARPES measurement result.[15] Note that a single isotropic energy gap cannot reproduce the conductivity spectrum at 6 K as displayed in the inset of Fig. 2. The two energy gaps reflect the multiband nature of the iron-based superconducting compounds. However, the infrared technique cannot distinguish between the $s^{\pm}$ and the nodeless s wave gaps. Recently, Pimenov *et al.*[16] measured the conductivity of $FeSe_{0.5}Te_{0.5}$ superconducting

films in the terahertz frequency range using backward-wave-oscillator spectroscopy. In the superconducting state, the real part of the complex conductivity remains finite, indicating the existence of a very strong anisotropic gap, the smaller one of the two gaps is estimated to be close to 12 cm^{-1} (1.5 meV).

The infrared spectroscopy study of the inter-plane electronic response was reported by Moon *et al.* for the $FeTe_{0.55}Se_{0.45}$ crystals (Fig. 4).[17] The *ab*-plane and the *c*-axis optical reflectance spectra are shown in Fig. 4(a). Although the electronic background is identified by the up-turn on $R_c(\omega)$ in the far-infrared region, it is still strongly suppressed as compared with the *ab*-plane response. In spite of the relatively low anisotropic ratio of in-plane conductivity over *c*-axis conductivity, the out-of-plane optical response is rather incoherent. In Fig. 4(b), $\sigma_c(\omega)$ does not show a well-defined Drude peak at all temperatures. The $\sigma_c(\omega)$ is continuously suppressed with decreasing T, and the suppressed spectral weight is not recovered up to 5000 cm^{-1}, as shown in the inset. The spectral weight transfer from low frequency to high frequency implies the presence of *c*-axis pseudogap, and the unexpected high energy scale of spectral weight redistribution is regarded as a spectroscopic hallmark of the strong electronic correlation.

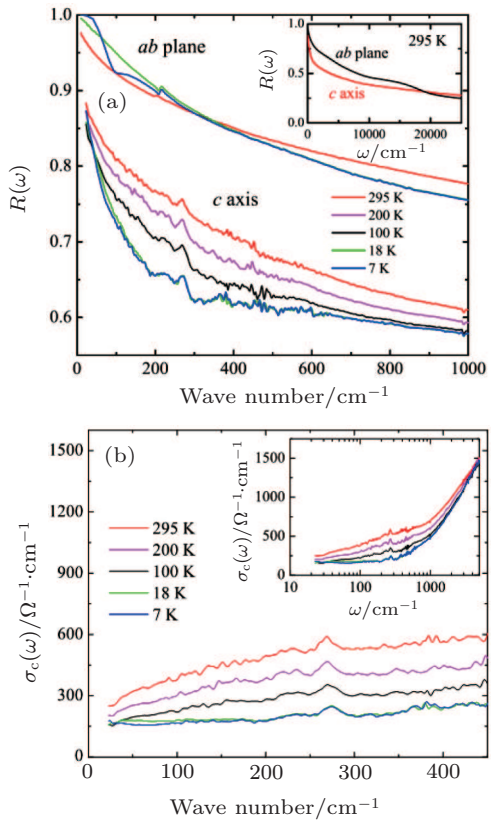


Fig. 4. (a) The T-dependent *c*-axis reflectance $R_c(\omega)$ of $FeTe_{0.55}Se_{0.45}$ with $T_c = 14$ K. The *ab*-plane reflectance $R_{ab}(\omega)$ is also plotted for comparison. (b) The T-dependent *c*-axis optical conductivity $\sigma_c(\omega)$ for $FeTe_{0.55}Se_{0.45}$.[17]

A comparison of the charge dynamics of $Fe_{1.087}Te$ and $SrFe_2As_2$ across the structural/magnetic transitions was reported by Hancock *et al.*[18] The two systems have different antiferromagnetic patterns below the magnetic transition temperatures, collinear AFM order for 122 and bicollinear AFM order for 11, as displayed in Fig. 5. The magnetic Brillioun zones are shown in Figs. 5(c) and 5(d). In the 122 system, the magnetic phase shows decreased plasma frequency and scattering, associated with the appearance of strong midinfrared features. The 11 system also shows a decreased scattering, but an increase in the plasma frequency, while no clear midinfrared features appear below the ordering temperature. The marked contrast is interpreted in terms of the different magnetic-ordering patterns of the ground states. The collinear AFM order results in the band folding between Γ and M points in the Brillouin zone, leading to the SDW gap opening due to the mixing electron and hole bands in the 122 system, whereas the folding by the bicollinear AFM order is between M and X points, which does not lead to the mixing of the electron and hole bands in the 11 based system.

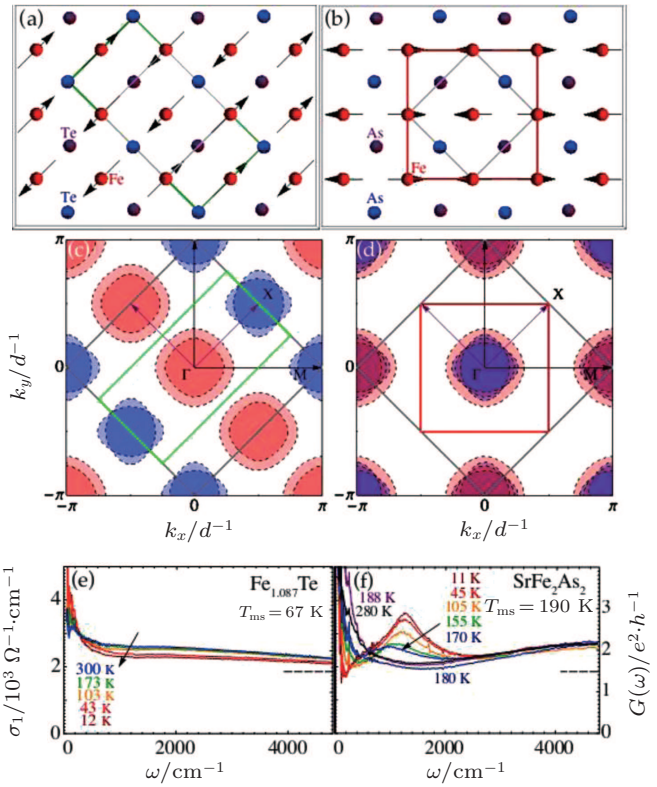


Fig. 5. Low-temperature magnetic structures of (a) $Fe_{1.087}Te$ and (b) $SrFe_2As_2$. (c) and (d) Fermi-surface folding expected from the lowered structural/magnetic symmetry. Optical conductivity of (e) $Fe_{1.087}Te$ and (f) $SrFe_2As_2$ at different temperatures.[18]

Theoretical calculations indicated that pure FeSe has a two-dimensional electronic structure similar to that of the Fe pnictides with cylindrical electron sections at the zone corner and hole sections at the zone center. Therefore, a similar SDW order with a collinear antiferromagnetic structure was predicted. Although no experimental evidence for the presence of

such an SDW order was found in earlier experiments on polycrystalline samples, a very recent ARPES measurement[19] on FeSe thin films indicated that, except for the single layered FeSe film, the band structure near the Brillouin zone corner at low temperature is very similar to that observed for the parent compounds of the FeAs-based systems, e.g., $BaFe_2As_2$ and NaFeAs in the SDW state. The phenomenon was suggested to arise from the formation of the collinear antiferromagnetic structure. However, unlike $BaFe_2As_2$ compound, no clear folding effect between Γ and M points in the Brillouin zone was observed. The emergence of gap-like excitation at low temperature was also found in earlier transient optical pump–probe measurement on the FeSe film.[20] The experiment revealed the presence of an additional sub-ps relaxation below roughly 130–140 K after pump (Fig. 6), which was suggested to be associated with the nematicity-induced short-range charge and/or orbital ordering in FeSe.

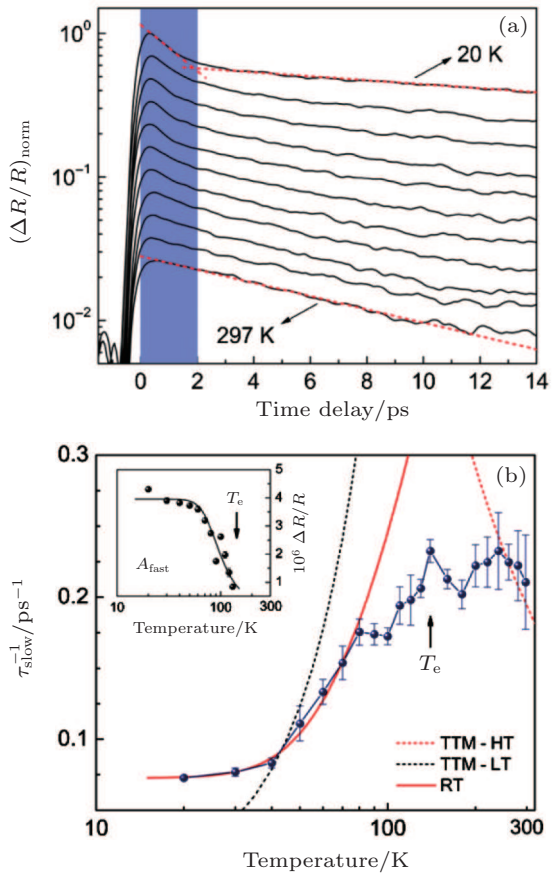


Fig. 6. (a) Temperature dependence of picosecond response of transient optical reflectivity $\Delta R/R$. The data are normalized and vertically shifted for clarity. (b) The T-dependent $\tau_{\rm slow}^{-1}$ and (inset) $A_{\rm fast}$.[20]

Nevertheless, the determination of the energy gap from the above measurement is indirect, which is different from the infrared spectroscopy technique in the equilibrium state. Yuan *et al.* reported an in-plane optical spectroscopy measurement on the (00l) FeSe thin film grown on $SrTiO_3$ substrate (Fig. 7).[21] From the inset of Fig. 7, the line shape of $\sigma_1(\omega)$ of the FeSe film is similar to that of $BaFe_2As_2$. However, the low-frequency conductivity $\sigma_1(\omega)$ is smaller than that in iron-pnictides 122 compound, implying a smaller plasma frequency. Comparing with the density function calculations, a stronger correlation effect is obtained. Figures 7(a) and 7(b) display the $\sigma_1(\omega)$ spectra up to 8000 cm^{-1} and 500 cm^{-1}, respectively. Similar to iron pnictides, a temperature-induced spectral weight transfer from low frequency to high frequency (roughly above 3500 cm^{-1}) is observed for FeSe, though the relevant energy scale is smaller. Such a spectral change represents the redistribution of the spectral weight between different 3d bands. Hund's coupling between itinerant electrons and more localized electrons of Fe 3d orbitals plays the major role here. More significantly, the measurement does not reveal any signature of SDW energy gap formation or band structure reconstruction. This suggests an absence of the static SDW order in FeSe. The gap-like reconstruction or relaxation seen by ARPES or pump–probe measurements may reflect very short life-time SDW fluctuations present in their samples.

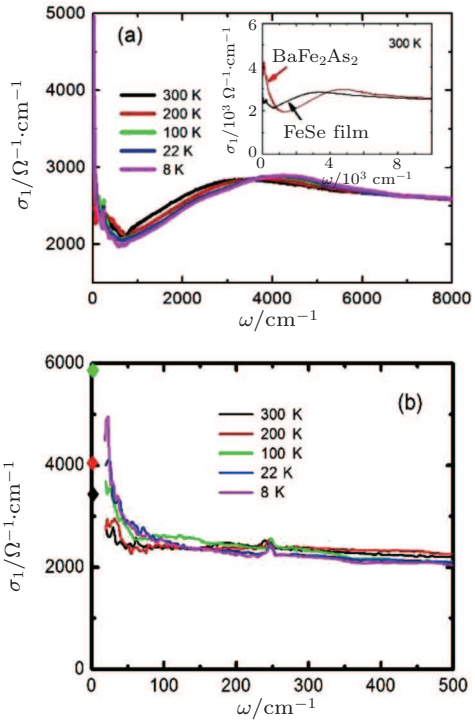


Fig. 7. (a) Conductivity spectra $\sigma_1(\omega)$ of FeSe film at different temperatures. Inset: the comparison of $\sigma_1(\omega)$ with $BaFe_2As_2$. (b) Detailed plot of $\sigma_1(\omega)$.[21]

3. $A_xFe_{2-y}Se_2$

The discovery of the Fe-selenide superconductors $A_xFe_{2-y}Se_2$ (A = K, Cs, Rb, Tl) has attracted a lot of attention because they behave quite differently compared with iron-pnictide superconductors.[6] Muon-spin relaxation (μSR), neutron diffraction, resistivity, and magnetization measurements on $A_xFe_{2-y}Se_2$ indicated a coexistence of superconductivity with a strong AFM order. In particular, the neutron

experiments revealed a blocked checkerboard antiferromagnetism for the system. Chen *et al*. performed an infrared spectroscopy measurement on $K_{0.83}Fe_{1.53}Se_2$ (Fig. 8),[22] a semiconducting parent compound of the iron selenide superconductors. The reduction of the low-frequency $R(\omega)$ with decreasing temperature suggests a semiconducting or insulating behavior. Correspondingly, there is no Drude-like response at low frequency in the conductivity spectra. From the extrapolation of the major absorption peak, a direct energy gap of 0.37 eV is identified. In comparison with the band structure calculation,[23] the insulating response could be attributed to the K-245 phase, which is the majority phase. Below the threshold, a weak absorption still exists. Another energy gap rough about 30 meV (250 cm^{-1}) could be identified, which could be attribute to another semiconducting phase K-234.[24]

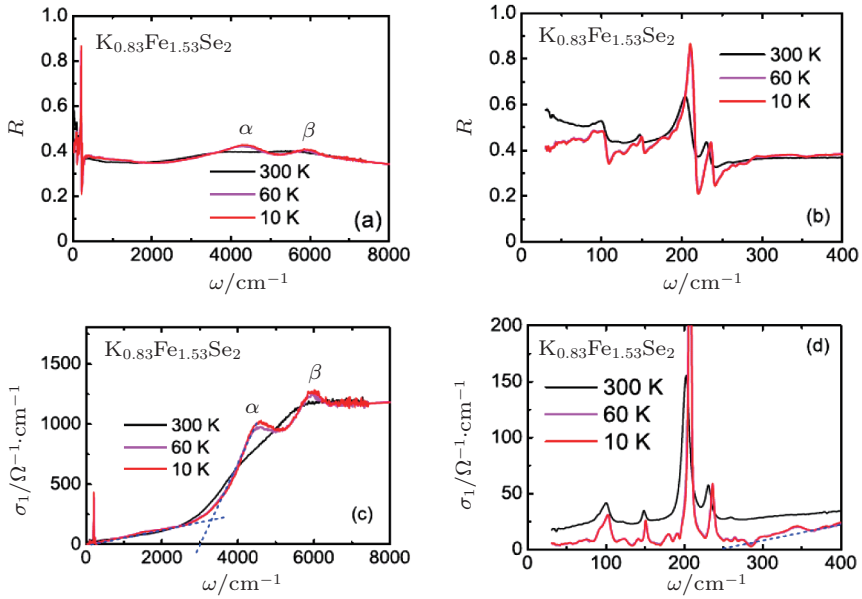


Fig. 8. (a) Optical reflectance $R(\omega)$ spectra at different temperatures up to 8000 cm^{-1}. (b) An expanded plot of $R(\omega)$ spectra below 400 cm^{-1}. (c) Conductivity $\sigma_1(\omega)$ spectra of the sample at different temperatures up to 8000 cm^{-1}. (d) An expanded plot of $\sigma_1(\omega)$ spectra below 400 cm^{-1}. The dashed straight lines are used for the extrapolation of energy gaps.[22]

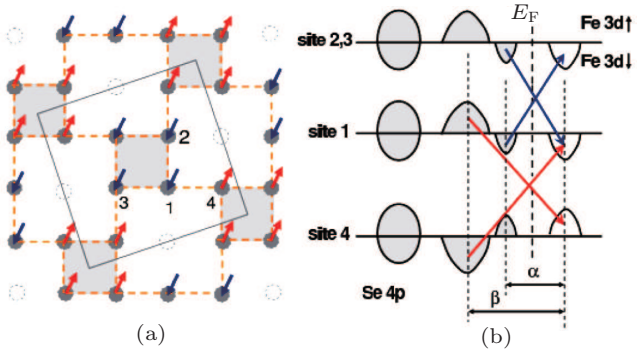


Fig. 9. (a) Magnetic structure determined by the neutron-diffraction experiment. (b) Schematic picture for the band occupation of each Fe site.[22]

Besides the semiconducting/insulating response, the measurement revealed two peculiar spectral structures: double interband transition peaks in the mid- to near-infrared region (4000 cm^{-1})–6000 cm^{-1}) and abundant phonon modes below 400 cm^{-1}. The two peculiar features have been thoroughly analyzed and explained in terms of the coexistence of ferromagnetic and antiferromagnetic couplings between the neighboring Fe sites. In this block AFM state, each Fe site is ferromagnetic coupled with two neighboring Fe sites and antiferromagnetic coupled with the third neighboring Fe site (Fig. 9). Site 4 has opposite spin-polarized occupations with sites 1, 2, and 3. Possible transitions are indicated by the arrows. It should be noticed that, although the d–d transitions are forbidden in an atom, such transitions become plausible through p–d hybridizations in solids. The double peaks represent the coexistence of the ferromagnetic and antiferromagnetic correlations between the neighboring sites. The double peaks reflect the coexistence of ferromagnetic and antiferromagnetic couplings between the neighboring Fe sites.

The optical response of a superconducting single crystal $K_{0.75}Fe_{1.75}Se_2$ was first studied by Yuan *et al*.[25] The study revealed peculiar spectral features in the superconducting state, which they attributed to the nanoscale phase separation between antiferromagnetic order and superconducting phase. As shown in Fig. 10, the reflectance over broad frequencies is rather low, roughly below the value of 0.4, being similar to the insulating compound with a lower Fe content. The double-peak absorption structure between 4000 cm^{-1} and 6000 cm^{-1} and the abundant phonon peaks are also present in the superconducting crystals, suggesting the presence of Fe vacancies and their orderings. The presence of the $\sqrt{5} \times \sqrt{5} \times 1$ superstructure modulation was indeed identified by the transmission

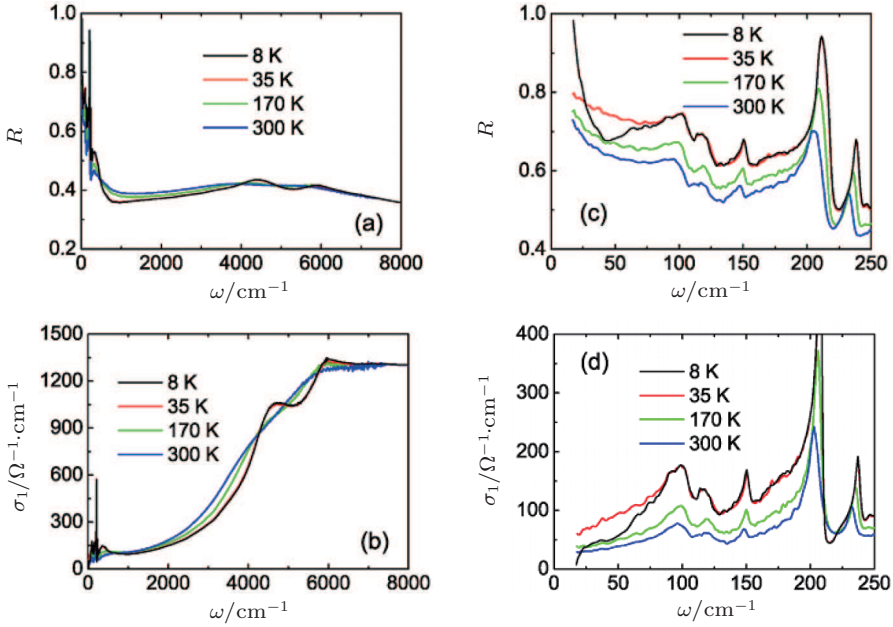


Fig. 10. (a) and (b) Optical reflectance $R(\omega)$ and conductivity $\sigma_1(\omega)$ spectra at different temperatures up to 8000 cm^{-1}. (c) and (d) Expanded plots of $R(\omega)$ and $\sigma_1(\omega)$ spectra below 250 cm^{-1}. A sharp plasma edge in $R(\omega)$ develops at low frequency in the superconducting state.[25]

electron microscopy (TEM) measurement (Fig. 11). However, in the superconducting state, a sharp reflectance edge was found at a rather low frequency. Yuan *et al*. elaborated that this sharp feature is unlikely caused by the formation of the superconducting energy gap, instead they attributed it to the Josephson-coupling plasma mode arising from the superconducting condensate.

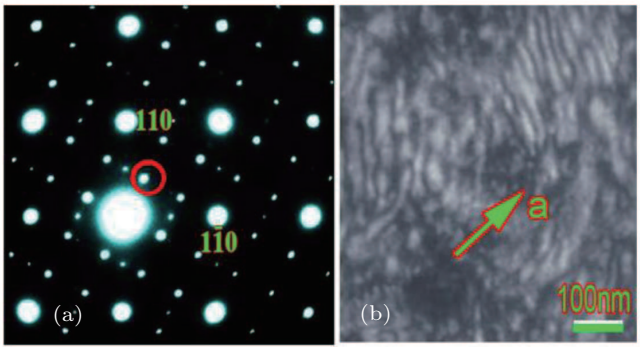


Fig. 11. Phase separation in a $K_{0.75}Fe_{1.75}Se_2$ superconducting crystal. (a) Electron diffraction pattern showing the presence of superstructure spots along the [310] direction, the cycled spot is used for dark-field imaging. (b) Dark field image taken from a thin region of the crystal. Stripe-type phase separation can be directly observed. The arrow indicates the [100] direction.[25]

In order to directly check the proposal, Yuan *et al*. carried out TEM investigations at room temperature, as shown in Fig. 11. The dark field image taken from the red-circle region is shown in Fig. 11(b). This kind of complex contrast in Fig. 11(b) can be explained directly as the coexistence of Fe-vacancy ordered areas and Fe-disordered areas (metallic/superconducting phase). The length of a stripe appears in the range from several to several tens or even over 100 nm, while its width is usually less than 10 nm. The combined optical and TEM studies provide a compelling evidence for the presence of nanoscale phase separation between superconductivity and magnetism.

Homes *et al*.[26] also studied the optical response of a superconducting $K_{0.8}Fe_{2-y}Se_2$ crystal. The extracted superfluid density follows the scaling line $\rho_{s0}/8 \propto 4.4\sigma_{dc}T_c$ (Fig. 12) in a region associated with the Josephson coupling. They concluded that this material is inhomogeneous and constitutes Josephson couplings. They also modeled the normal state of $K_{0.8}Fe_{2-y}Se_2$ using the Bruggeman effective medium approximation (B-EMA) for metallic inclusions in an insulating matrix. They estimated that about 10% of the total sample volume is metallic. The result is consistent with the earlier studies.

Similar results were also obtained for $K_{0.73}Fe_{1.67}Se_2$ with $T_c = 32$ K by Wang *et al*. (Fig. 13).[27] They performed both μSR and infrared spectroscopy measurements. The combined experiments can be consistently described in terms of a macroscopically phase segregated state with a matrix of $\sim 88\%$ volume fraction that is insulating and strongly magnetic and inclusions with a $\sim 12\%$ volume fraction which are metallic, superconducting, and non-magnetic. The analysis of the infrared data with a model based on the effective medium approximation (EMA) revealed that the metallic inclusions have an elongated, almost needle-like shape and the percolation between them is achieved in most of the sample volume. Figure 13 shows the fitting of the normal state spectra using the EMA model. The resulting total unscreened plasma frequency of the two Drude components, $\omega_{p,D} \approx 5000$ cm^{-1}, appears to be similar or on the same order of magnitude as in other iron selenide or arsenide superconductors.

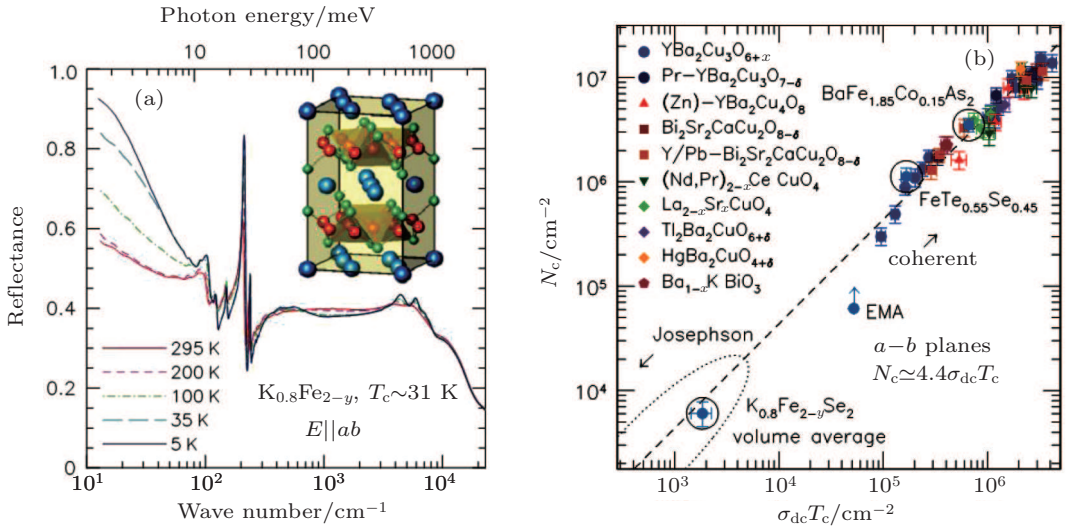


Fig. 12. (a) Optical reflectance at different temperatures for $K_{0.8}Fe_{2-y}Se_2$. Inset: structure of $K_{0.8}Fe_{2-y}Se_2$. (b) The log–log plot of $N_c = \rho_{s0}/8$ versus $\sigma_{dc}T_c$ in the *ab* planes for a variety of cuprate superconductors as well as several iron-based superconductors compared with the volume-average and EMA results for $K_{0.8}Fe_{2-y}Se_2$.[26]

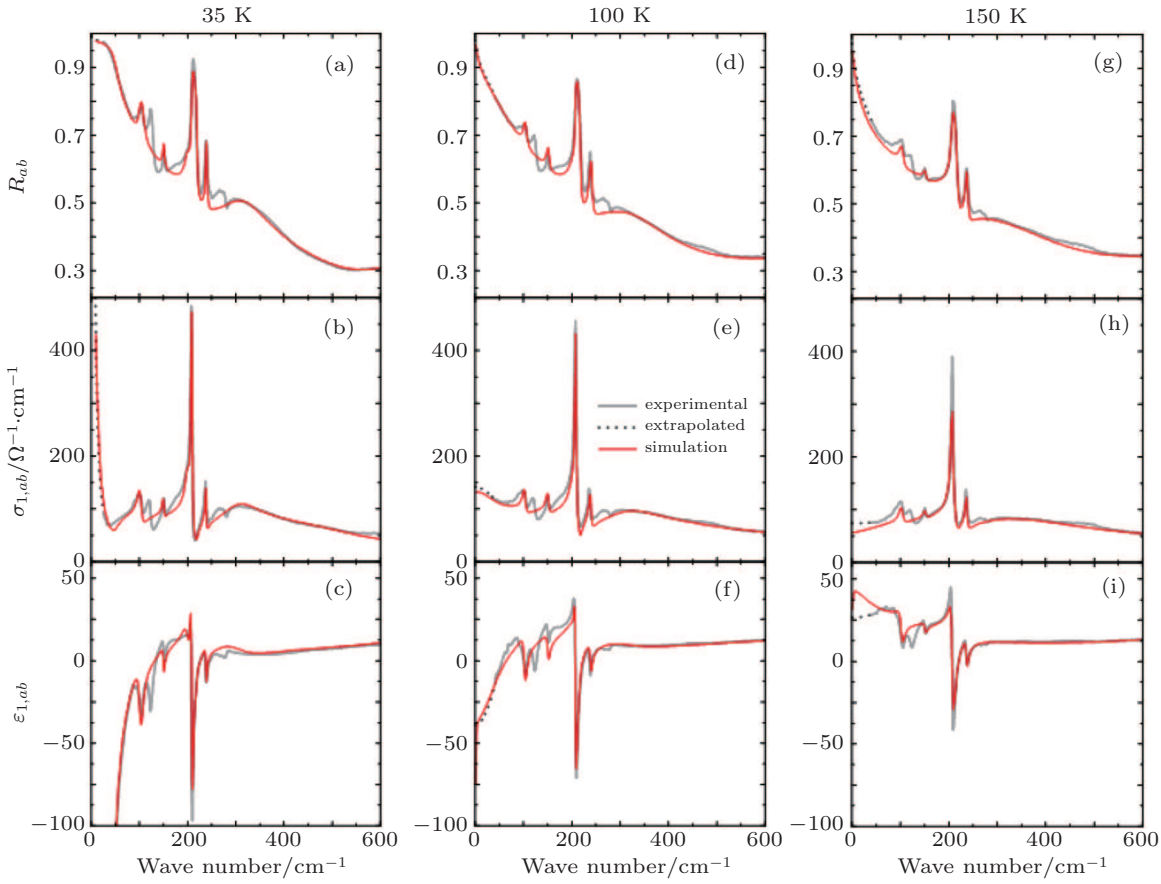


Fig. 13. Comparison of the experimental data in the normal state of KFS_SC with the fits based on the EMA model.[27]

Due to the fact that only electron pockets are present in $A_xFe_{2-y}Se_2$, the nesting scenario, which is applied to other iron selenide or arsenide superconductors, becomes apparently invalid. It is interesting to examine the evolution of the electronic structure across the AFM transition in the $A_xFe_{2-y}Se_2$ compound. $Cs_{0.8}(Fe_{1.05}Se)_2$ with a relatively high Néel temperature ($T_N = 492$ K) was studied by optical spectroscopy (Fig. 14). The optical measurement was performed in the temperature range from 10 K up to 500 K.[28] The low-frequency optical response shows an insulating behavior, with a major

absorption near 0.31 eV. The double-peak structure in the mid-infrared region and the low-frequency phonon modes support the presence of the blocked anti-ferromagnetism. The study clearly illustrates the absence of SDW energy gap formation after the AFM transition, indicating that the electronic state below the AFM transition is almost the same as that above the transition. The magnetic transition is more similar to the disorder–order phase transition, which is due to the local moment exchange interaction.

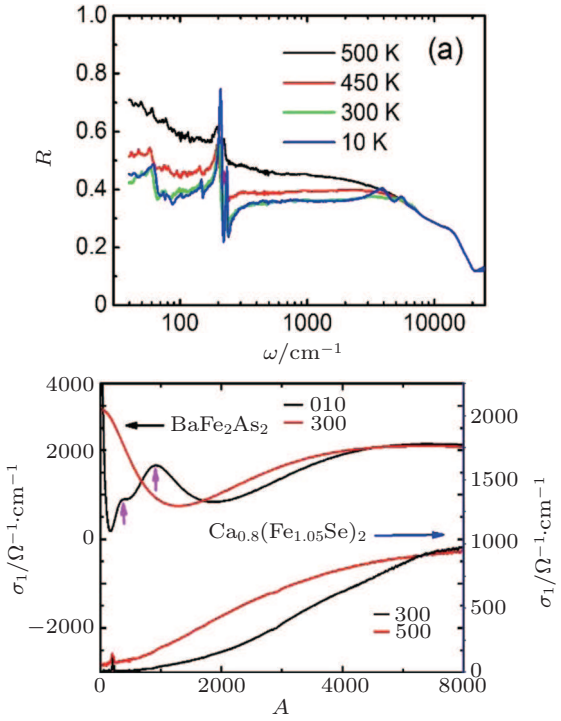


Fig. 14. (a) Optical reflectance $R(\omega)$ spectra at different temperatures. (b) Conductivity of $Cs_{0.8}(Fe_{1.05}Se)_2$ comparing with that of $BaFe_2As_2$ up to 6000 cm^{-1}.[28]

4. Conclusion

To summarize, optical measurements have provided fruitful information about the band structure evolution across the AFM phase transition temperature, the correlation effect, the superconducting pairing energy gap, the condensed carrier density or penetration depth, the inhomogeneity and the nanoscale phase separation between superconductivity and antiferromagnetism in Fe-selenide superconducting systems. Nevertheless, some issues remain to be resolved with respect to the optical investigations. For example, although the temperature-induced spectral weight transfer from low frequency to high frequency was attributed to the redistribution of electronic spectral weight within different Fe 3d orbitals, the difference of energy scales between different systems needs to be further addressed. It is believed that such a study would shed new light on the electronic correlation effect in Fe-based superconductors.

References

[1] Kamihara T W, Hirano M and Hosono H 2008 *J. Am. Chem. Soc.* **130** 3296

[2] Hsu F C, Luo J Y, Yeh K W, Chen T K, Huang T W, Wu P M, Lee Y C, Huang Y L, Chu Y Y, Yan D C and Wu M K 2008 *Proc. Natl. Acad. Sci. USA* **105** 14262

[3] Wu M K, Hsu F C, Yeh K W, Huang T W, Luo J Y, Wang M J, Chang H H, Chen T K, Rao S M, Mok B H, Chen C L, Huang Y L, Ke C T, Wu P M, Chang A M, Wu C T and Perng T P 2009 *Physica C* **469** 340

[4] Medvedev S, McQueen T M, Troyan I A, Palasyuk T, Eremets M I, Cava R J, Naghavi S, Casper F, Ksenofontov V, Wortmann G and Felser C 2009 *Nat. Mater.* **8** 630

[5] Wang Q Y, Li Z, Zhang W H, Zhang Z C, Zhang J S, Li W, Ding H, Ou Y B, Deng P, Chang K, Wen J, Song C L, He K, Jia J F, Ji S H, Wang Y Y, Wang L L, Chen X, Ma X C and Xue Q K 2012 *Chin. Phys. Lett.* **29** 037402

[6] Guo J G, Jin S F, Wang G, Wang S C, Zhu K X, Zhou T T, He M and Chen X L 2010 *Phys. Rev. B* **82** 180520

[7] Sun L, Chen X J, Guo J, Gao P, Huang Q Z, Wang H, Fang M, Chen X, Chen G, Wu Q, Zhang C, Gu D, Dong X, Wang L, Yang K, Li A, Dai X, Mao H K and Zhao Z 2012 *Nature* **483** 67

[8] Fang M H, Wang H D, Dong C H, Li Z J, Feng C M, Chen J and Yuan H Q 2011 *Europhys. Lett.* **94** 27009

[9] Bao W, Huang Q Z Chen G F, Green M A, Wang D M, He J B and Qiu Y M 2011 *Chin. Phys. Lett.* **28** 086104

[10] Zhang Y, Yang L X, Xu M, Ye Z R, Chen F, He C, Xu H C, Jiang J, Xie B P, Ying J J, Wang X F, Chen X H, Hu J P, Matsunami M, Kimura S and Feng D L 2011 *Nat. Mater.* **10** 273

[11] Chen G F, Chen Z G, Dong J, Hu W Z, Li G, Zhang X D, Zheng P, Luo J L and Wang N L 2009 *Phys. Rev. B* **79** 140509

[12] Hu W Z, Dong J, Li G, Li Z, Zheng P, Chen G F, Luo J L and Wang N L 2008 *Phys. Rev. Lett.* **101** 257005

[13] Xia Y, Qian D, Wray L, Hsieh D, Chen G F, Luo J L, Wang N L and Hasan M Z 2009 *Phys. Rev. Lett.* **103** 037002

[14] Homes A A, Wen J S, Xu Z J, Lin Z W, Li Q and Gu G D 2010 *Phys. Rev. B* **81** 180508

[15] Miao H, Richard P, Tanaka Y, Nakayama K, Qian T, Umezawa K, Sato T, Xu Y M, Shi Y B, Xu N, Wang X P, Zhang P, Yang H B, Xu Z J, Wen J S, Gu G D, Dai X, Hu J P, Takahashi T and Ding H 2012 *Phys. Rev. B* **85** 094506

[16] Pimenov A, Engelbrecht S, Shuvaev A M, Jin B B, Wu P H, Xu B, Cao L X and Schachinger E 2013 *New J. Phys.* **15** 13032

[17] Moon S J, Homes C C, Akrap A, Xu Z J, Wen J S, Lin Z W, Li Q, Gu G D and Basov D N 2011 *Phys. Rev. Lett.* **106** 217001

[18] Hancock J N, Mirzaei S I, Gillett J, Sebastian S E, Teyssier J, Viennois R, Giannini E and van der Marel D 2010 *Phys. Rev. B* **82** 014523

[19] Tan S Y, Xia M, Zhang Y, Ye Z R, Chen F, Xie X, Peng R, Xu D F, Fan Q, Xu H, Jiang J, Zhang T, Lai X C, Xiang T, Hu J P, Xie B P and Feng D L 2013 arXiv:1301.2748

[20] Wen Y C, Wang K J, Chang H H, Luo J Y, Shen C C, Liu H L, Sun C K, Wang M J and Wu M K 2012 *Phys. Rev. Lett.* **108** 267002

[21] Yuan R H, Kong W D, Yan L, Ding H and Wang N L 2013 *Phys. Rev. B* **87** 144517

[22] Chen Z G, Yuan R H, Dong T, Xu G, Shi Y G, Zheng P, Luo J L, Guo J G, Chen X L and Wang N L 2011 *Phys. Rev. B* **83** 220507

[23] Cao C and Dai J 2011 *Phys. Rev. Lett.* **107** 056401

[24] Yan X W, Gao M, Lu Z Y and Xiang T 2011 *Phys. Rev. Lett.* **106** 087005

[25] Yuan R H, Dong T, Song Y J, Zheng P, Chen G F, Hu J P, Li J Q and Wang N L 2012 *Sci. Rep.* **2** 221

[26] Homes C C, Xu Z J, Wen J S and Gu G D 2012 *Phys. Rev. B* **85** 180510

[27] Wang C N, Marsik P, Schuster R, Dubroka A, Rösle M, Niedermayer C, Varma G D, Wang A F, Chen X H, Wolf T and Bernhard C 2012 *Phys. Rev. B* **85** 214503

[28] Yuan R H, Dong T and Wang N L 2013 *Chin. Phys. Lett.* **30** 077403